facilitating comparison of the lift curves for the various configurations. Up to lift coefficients of approximately unity, the two sets of data in Fig. 3a are remarkably similar with the two baseline configurations as well as the two configurations with fully extended Gurney flaps (4.5 ft in Ref. 1 and solid in Ref. 2), depicting nearly identical lift-curve slopes. The values for the maximum lift coefficient are shown to differ; however, the maximum increment in $C_{L_{max}}$ caused by the addition of the Gurney flap is, again, remarkably similar for both sets of data ($\Delta C_{L_{max}} = 0.3$). Note that the shift in the zero-lift angle of attack α_0 from the baseline caused by the fully extended (4.5 ft) flap, is -2.32 deg in Ref. 1 whereas the shift from the baseline caused by the fully extended (solid) flap is slightly less at -2.18 deg in Ref. 2. There is a very noticeable steepening of the lift curve slope because of the trailing-edge modifications for angles of attack up to ~ 10 deg. This steepening is the result of an apparent nonlinear change in effectiveness of the flap as a function of angle of attack, which is also observed in two-dimensional wind-tunnel experiments for the NLF(1)-0414F airfoil. In Fig. 4, the two-dimensional results by McGhee et al.[4] measured at a Reynolds number of 3.0×10^6 for a $0.0125c$ Gurney flap (reported in Ref. 5), and the three-dimensional results of Ref. 2 show a very similar change in α_0 and lift-curve slope. Hence, the steepening in the lift-curve slope caused by the trailing-edge modification appears to be two dimensional in nature.

In Fig. 3b, the effects of the trailing-edge modifications on the aerodynamic performance parameter, L/D, are presented. For both sets of data, the trailing-edge modifications result in a shift of C_L for $(L/D)_{max}$ to higher lift coefficients. However, for the configurations of Ref. 1, $(L/D)_{max}$ is shown to drop with increasing extent of the Gurney flap, whereas an increase in $(L/D)_{max}$ is shown for the configurations of Ref. 2. This discrepancy is likely linked to 1) the effect of the trailing-edge modification on boundary-layer transition, which was kept free in Ref. 1 and fixed near the leading-edge in Ref. 2; and 2) the size of the Gurney flap that is $0.033c$ in Ref. 1 and $0.015c_{ref}$ in Ref. 2. The Gurney flap changes the pressure distribution in such a manner that transition on the upper surface of the NLF(1)-0414F occurs naturally near the leading edge, even at low lift coefficients (see Figs. 4 and 5 of Ref. 5), resulting in a drag penalty for laminar-flow lifting surfaces. The larger flap size does little to further enhance the lift as demonstrated in Fig. 2a, but has a severely adverse effect on the drag. By comparison, note the beneficial effect of the serrated shape of the trailing-edge modification on the performance characteristics; L/D is better than the baseline wing for $C_L > 0.4$ and, unlike the solid flap, there is little or no L/D penalty at lower lift coefficients. The advantages of the serrated flap over the solid flap are as follows:

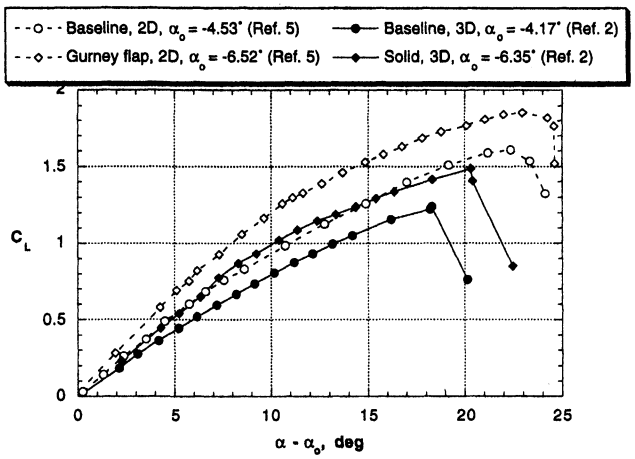

Fig. 4 Comparison of two-dimensional vs three-dimensional effect of Gurney-flap trailing-edge modification on lift of NLF(1)-0414F.

1) For a given lift increment, the spanwise load distribution, and hence, induced drag, may be less severely affected by a full-span serrated flap as compared with a part-span solid flap.

2) The streamwise vorticity created by the serrations may reduce or eliminate flow separation in the trailing-edge region as explained in more detail in Ref. 2.

Finally, Ref. 2 presents the effects of Gurney-flap additions on nose-down pitching moment (not shown in Ref. 1), requiring the consideration of trim-drag implications.

Concluding Remarks

The results of Refs. 1 and 2, both at a Reynolds number of approximately 1×10^6, are largely in agreement in terms of the overall effect of Gurney flaps on the lift characteristics of wings. However, the larger solid flaps tested in Ref. 1 provide little additional lift benefit while negatively affecting the drag. In comparison, the $0.015c_{ref}$ Gurneys in Ref. 2 allow an increase in $(L/D)_{max}$ of $\sim 6\%$. Maybe the most important observation is that continuous Gurney flaps are not required to be effective on three-dimensional configurations. As shown, spanwise variations in the flap geometry, such as serrations, allow modulation of the lift increment without accruing (severe) drag penalties.

References

[1]Myose, R., Papadakis, M., and Heron, I., "Gurney Flap Experiments on Airfoils, Wings, and Reflection Plane Model," *Journal of Aircraft*, Vol. 35, No. 2, 1998, pp. 206–211.

[2]Vijgen, P. M. H. W., van Dam, C. P., Holmes, B. J., and Howard, F. G., "Wind-Tunnel Investigations of Wings with Serrated Sharp Trailing Edges," *Low Reynolds Number Aerodynamics*, edited by T. J. Mueller, Vol. 54, Lecture Notes in Engineering, Springer–Verlag, New York, 1989, pp. 295–313.

[3]Vijgen, P. M. H. W., Howard, F. G., Bushnell, D. M., and Holmes, B. J., "Serrated Trailing Edges for Improving Lift and Drag Characteristics of Lifting Surfaces," US Patent 5,088,665, Feb. 18, 1992 (Invention Disclosure LAR 13870-1-CU, Aug. 31, 1987).

[4]McGhee, R. J., Viken, J. K., Pfenninger, W., Beasley, W. D., and Harvey, W. D., "Experimental Results for a Flapped Natural-Laminar-Flow Airfoil with High Lift/Drag Ratio," NASA TM 85788, May 1984.

[5]Neuhart, D. H., and Pendergraft, O. C., Jr., "A Water Tunnel Study of Gurney Flaps," NASA TM 4071, Nov. 1988.

Flowfield Simulation About a 65-Degree Delta Wing During Constant Roll-Rate Motions

Jeffrey C. Tromp*
U.S. Air Force Research Laboratory, Wright–Patterson Air Force Base, Ohio 45433-7521

Introduction

THE effects of roll and yaw rates on aerodynamic reactions and vortex breakdown locations for a 65-deg delta wing are described. Two distinct maneuvers are numerically simulated to isolate the rate effects. The first is a constant-rate coning motion, with computed body-axis moments compared with

Presented as Paper 98-4453 at the AIAA Atmospheric Flight Mechanics Conference, Boston, MA, Aug. 10–12, 1998; received Oct. 21, 1998; accepted for publication Nov. 3, 1998.

*Aerospace Engineer, AFRL/VAAC, Building 146, 2210 Eighth Street, Suite 11. Senior Member AIAA.

rotary data from the U.S. Air Force Research Laboratory (AFRL) vertical wind tunnel. The second is a constant-roll-rate, barrel-roll maneuver with zero pitch and yaw rates. In both maneuvers, the angle of attack and sideslip angle are fixed at 30 and 0 deg, respectively. This study is motivated by recent efforts[1,2] to model the nonlinear, unsteady aerodynamics of the rolling 65-deg delta wing, including the effects of crossing critical states,[1] which are states where bifurcations occur in the static aerodynamic responses.

The rate effect on breakdown location is of particular interest because some critical states appear to correspond to a discontinuous jump in breakdown location, such as the case near 5-deg body-axis roll angle and 30-deg angle of attack.[1] It is currently unknown, however, if this or other critical-state locations are sensitive to vehicle angular rates. This work only begins to answer this question by quantifying rate effects on breakdown for the zero-sideslip case.

Experimental results from rotary testing may be helpful in determining rate effects. However, for nonzero angles of attack, coning motions also produce a yaw rate. Thus, isolating the effects of roll and yaw rates helps determine the utility of using coning data to estimate certain critical-state rate effects. The coning motion is prescribed by aligning the vehicle rotation vector with the freestream. The wing rotates about the c.g., which is 57% aft of the apex along the wing centerline. The coning motion (subscript c), for zero body-axis roll angle, produces body-axis rates,[3] $p_c = \Omega \cos \alpha = \Omega U_c$, $q_c = V_c = 0$, and $r_c = \Omega \sin \alpha = \Omega W_c$, where Ω is the coning rate nondimensionalized by root chord and freestream velocity, U_{ref}, α is the angle of attack, and U_c, V_c, W_c are the body-axis velocity components normalized by U_{ref}. The helical motion (subscript h) is prescribed by a constant body-axis roll such that $p_h = p_c = \Omega \cos \alpha$ and $q_h = r_h = 0$. Body-axis velocity components U_h, V_h, W_h are chosen to match those of the coning motion, i.e., $U_h = U_c = \cos \alpha$, $V_h = V_c = 0$, and $W_h = W_c = \sin \alpha$. Thus, for nonzero α, the two motions differ only in the yaw rate. To achieve the desired rates for the helical motion, the c.g. is not fixed in inertial space. The c.g. trajectory can be found by resolving V_h and W_h onto an inertial system aligned with the body-axis crossflow plane and integrating, resulting in a circular path in a plane normal to the x-body axis with center at $y = -W_h/p_h$ and $z = V_h/p_h$. To avoid numerical errors caused by a step onset of rate, Ω is smoothly transitioned in the numerical simulations from zero to its final, constant value at $\bar{t} \equiv t/0.25 = 1$, using a transition function $\Omega_1(t) = \Omega(3\bar{t}^2 - 2\bar{t}^3)$. The time, t, is nondimensionalized by root chord and U_{ref}. Laminar numerical simulations for both maneuvers were performed for a Reynolds number based on root chord of 0.32×10^5 and a Mach number of 0.2. The Mach and Reynolds numbers were chosen for consistency with earlier static calculations over the same geometry,[4] thereby leveraging previous results of the necessary grid resolution. Wind-tunnel test conditions were different, with a Mach number of 0.025 and a Reynolds number of 0.35×10^6, based on a root chord of 2 ft. The 65-deg delta-wing geometry is depicted in Fig. 1. The

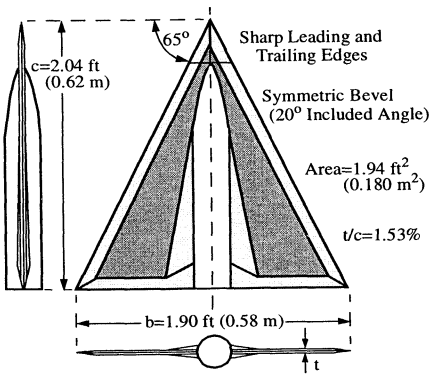

Fig. 1 Delta-wing model.

model has a sharp leading edge with upper and lower bevels, and a cylindrical centerbody with sting. The grid used is the baseline C–O topology grid used by Gordnier,[4] which consists of $317 \times 73 \times 143$ nodes in the circumferential, body normal, and axial directions.

A Beam–Warming[5] time-integration code, written by Visbal,[6] was employed to solve the unsteady, three-dimensional, full Navier–Stokes equations in strong conservation form using a general, time-dependent coordinate transformation. The code has been tested extensively for a variety of flows, including flows over a delta wing in pitch and roll, and flow over a pitching slender body of revolution (see Refs. 6 and 7). The flow solver is augmented for the current work to generate the two new maneuvers, to compute body-axis moment coefficients [based on wingspan, b, for rolling (C_l) and yawing (C_n) moments, and mean aerodynamic chord for pitching moment, C_m], and to compute the vortex-core and vortex-breakdown locations. Further details of the numerical simulations, along with a discussion of the grid and time-step requirements, are found in Ref. 8.

Results

Computations were performed for rates of $\bar{\Omega} = \Omega b/2U_{\text{ref}} = -0.05$, -0.10, and -0.20, noting that helical-motion roll rates are written in terms of the coning rate, Ω. A negative coning rate implies that the rotation vector points aft. The data were averaged after three time units ($t = 3$) elapsed from the start of the motion. This was done to exclude motion-startup transients from the computation of averages. Simulations were run out to 10–12 time units to achieve a sufficient data sample.

The excellent agreement between the time-averaged, body-axis moment coefficients for the coning-motion computations and the wind-tunnel results is shown in Fig. 2. Rolling moments match very well, with both the numerical and wind-tunnel experiments predicting an increase in rolling moment with negative coning rate. The agreement in pitching moment (about 35% mean aerodynamic chord) is also very good. The two experiments predict a small drop in pitching moment between coning rates of 0.00 and -0.10. Furthermore, both experiments also predict a large drop in pitching moment as the coning rate is increased from -0.10 to -0.20. Yawing moment appears to be nearly zero, and is virtually unaffected by the coning motion. The wind-tunnel results show a slightly nonzero yawing moment of $C_n = -0.0037$ under static conditions, which may be caused by a small bias in the wind-tunnel rig or balance instrumentation. Both experiments show, however, a slight increase in yawing moment at the highest coning rate. Numerical data values are shown in Table 1. The computed static pitching moment is 0.0284, whereas the wind-tunnel test indicated a static value of $C_m = 0.0253$.

Time-averaged moments resulting from the helical motion are shown in Table 2. As with the coning motion, yawing

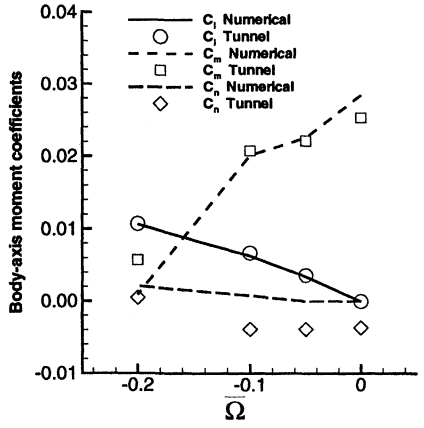

Fig. 2 Comparison between numerical computations and wind-tunnel results.

Table 1 Body-axis moments due to coning motion

	$\bar{\Omega} = -0.05$		$\bar{\Omega} = -0.10$		$\bar{\Omega} = -0.20$	
	CFD	Tunnel	CFD	Tunnel	CFD	Tunnel
C_l	0.0034	0.0036	0.0063	0.0067	0.0106	0.0107
C_m	0.0225	0.0221	0.0201	0.0207	0.0009	0.0057
C_n	0.0000	−0.0039	0.0008	−0.0039	0.0021	0.0005

Table 2 Body-axis moments due to helical motion

	p		
	−0.10	−0.20	−0.40
C_l	0.0081	0.0185	0.0359
C_m	0.0190	0.0211	0.0195
C_n	−0.0001	−0.0008	−0.0007

Table 3 Time-averaged breakdown locations and breakdown shift due to yaw rate

	Helical		Coning		Yaw-rate shift	
$\bar{\Omega}$	Left	Right	Left	Right	Left	Right
−0.05	0.271	0.226	0.241	0.287	−0.030	0.061
−0.10	0.287	0.250	0.236	0.378	−0.051	0.128

moment is virtually zero, and has almost no dependence on roll rate within the range of the data. Pitching moment is also nearly constant with roll rate. Rolling moment is found to vary quasilinearly with roll rate, with C_{l_p} found to be -0.09 rad^{-1}. This linearity is significant, because recent nonlinear modeling techniques[2] assume the linearity of rolling moment with roll rate. The helical motion provides a direct check of this assumption because it produces a constant roll rate while the body-axis roll angle is held fixed at zero. The modeling technique also benefits from direct knowledge of the total roll damping, because this reduces by one the number of unknowns to extract from a set of experimental data. Rolling moment due to yaw rate, C_{l_r}, can also be approximated assuming that roll- and yaw-rate effects can be superimposed. That is, the roll moment from the coning motion less the rolling moment from the helical motion yields rolling moment due to yaw rate, $C_{l_r} = 0.11$ rad^{-1}.

Breakdown locations, defined here as the most forward location of reversed flow, were visually checked by comparing them with the axial location of the most forward kink in computed vortex lines emanating near the apex.[8] The time-averaged axial locations for breakdown were computed for the two lowest rates, and shown in Table 3. Also shown are the changes in breakdown location caused by yaw rate, computed as the coning breakdown location minus the helical breakdown location. The time-averaged location for the static case was determined experimentally by Cipolla[9] to be 0.287 (or 28.7% of root chord from the apex), whereas computations on a fine grid by Gordnier[4] found it to be 0.288. Gordnier's computed location for the coarser grid used here was 0.295, only 2.5% higher. Increasing the roll rate for the helical motion had a small impact on breakdown location, with the left and right vortex breakdown locations moving slightly aft with increasing negative roll rate. For a given rate, the left breakdown location was only slightly farther aft than the right. For the coning motion, increasing the coning rate also had a small impact on the left vortex breakdown location. The largest impact was on the right vortex breakdown location, which moved aft only about 10% of chord between $\bar{\Omega} = -0.05$ and -0.10. The effect of yaw rate on breakdown location is computed from subtracting the location caused by the helical (roll-rate) motion from the location due to coning (roll and yaw rate). For a given rate, breakdown is farthest aft on the left side for the helical motion, but is farthest aft on the right side for the coning motion. That is, the effect of yaw rate is to switch the relative positions of breakdown. The effect of the negative yaw rate then is to move the left (windward) breakdown location forward, whereas the right position is moved aft. The negative yaw rate can be viewed as an effective decrease in the local sweep near the apex for the left side and an increase in local sweep on the right side. The effect of leading-edge sweep on delta-wing breakdown location was considered by Wentz and Kohlman,[10] who found that for a constant angle of attack, decreasing the leading-edge sweep effectively moves breakdown toward the apex, while increasing the sweep moves the breakdown aft. Thus, the shift in breakdown locations found here because of the yaw rate is in qualitative agreement with experimental evidence.

Changes in the lateral and normal positions of the prebreakdown, leading-edge vortex core were also recorded[8] and were found to be nearly time invariant. The only significant effect was a lateral movement caused by the coning motion, where the left/right vortex core moved quasilinearly inboard/outboard with higher negative rate.

Conclusions

Body-axis moments caused by coning are in excellent agreement with moments obtained from the AFRL's vertical wind-tunnel facility, suggesting that the grid resolution used in this study is adequate for determining vehicle forces and moments. The helical motion provides a direct means of computing the total roll damping, helping recent modeling efforts reduce by one the number of unknowns to extract from a set of experimental data. The change in the time-averaged breakdown locations due to rate were only on the order of 10% of root chord as rate was increased from $\bar{\Omega} = -0.05$ to -0.10. This suggests that some critical-state locations corresponding to jumps in breakdown location may not be greatly impacted by rate effects. Further computations at nonzero roll angles are needed to show this, however. For coning motions, the results indicate that the yaw rate effect on breakdown location is comparable in magnitude to the roll-rate effect.

References

[1]Jenkins, J. E., Myatt, J. H., and Hanff, E. S., "Body-Axis Rolling Motion Critical States of a 65-Degree Delta Wing," *Journal of Aircraft*, Vol. 33, No. 2, 1996, pp. 268–278.

[2]Myatt, J. H., "Modeling the Rolling 65-Degree Delta Wing with Critical State Encounters," AIAA Paper 97-3646, Aug. 1997.

[3]Orlik-Rückermann, K. J., "Rotary-Balance Testing for Aircraft Dynamics," AGARD, AR-265, 1990, p. 69.

[4]Gordnier, R. E., "Numerical Simulation of a 65-Degree Delta-Wing Flowfield," *Journal of Aircraft*, Vol. 33, No. 4, 1997, pp. 492–499.

[5]Beam, R. M., and Warming, R. F., "An Implicit Factored Scheme for the Compressible Navier-Stokes Equations," *AIAA Journal*, Vol. 16, No. 4, 1978, pp. 393–402.

[6]Visbal, M. R., "Numerical Investigation of Laminar Juncture Flows," AIAA Paper 89-1873, June 1989.

[7]Gordnier, R. E., "Computation of Delta-Wing Roll Maneuvers," *Journal of Aircraft*, Vol. 32, No. 3, 1995, pp. 486–492.

[8]Tromp, J. C., "Flowfield Simulation About a 65-Degree Delta Wing During Constant Roll-Rate Motions," AIAA Paper 98-4453, Aug. 1998.

[9]Cipolla, K. M., "Structure of the Flow Past a Delta Wing with Variations in Roll Angle," Ph.D. Dissertation, Dept. of Mechanical Engineering, Lehigh Univ., Bethlehem, PA, May 1996.

[10]Wentz, W. H., and Kohlman, D. L., "Vortex Breakdown on Slender Sharp-Edged Wings," *Journal of Aircraft*, Vol. 8, No. 3, 1971, pp. 156–161.